Opt Quant Electron (2017)49:51
DOI 10.1007/s11082-016-0886-2

Competitiveness of the BPM in studying the optical beams at critical incidence on dielectric interfaces

Lotfy R. Gomaa[1] · Adel Shaaban[2,3] · M. F. O. Hameed[2,4] · S. S. A. Obayya[2,4]

Received: 15 September 2016 / Accepted: 28 December 2016

Abstract We investigate the usefulness of the wide-angle Fast Fourier Transform-based beam propagation method (FFT-BPM) to investigate important and quite involved problems in the propagation of optical beams. The incident transverse electric (TE) and transverse magnetic (TM) optical beams at the critical angle on a dielectric interface are investigated. Major numerical difficulties associated with the singularity of the transverse derivative of the step-like refractive index at the interface plane (for the TM case) are circumvented via an "*equivalent-index*" formalism. An *arc-tangent* function is used to approximate the abrupt change of the refractive index at the interface, such that the singular derivative is eliminated, and the TM problem is transformed to an equivalent TE one with no singular behavior. Further, the propagation of a rectangular incident pulse on an interface at the critical angle is also studied. In this investigation, the large shift of the lateral field and the standing wave pattern resulting from the incident and reflected fields are investigated and justified by simple calculations. A new phenomenon, called "*spatial transient*" is discussed, concerning the substantial spatial evolution of the pulse over very short propagation distance (fraction of the wavelength). Finally, a parametric study of a

This article is part of the Topical Collection on Optical Wave and Waveguide Theory and Numerical Modelling 2016.

Guest edited by Krzysztof Anders, Xuesong Meng, Gregory Morozov, Sendy Phang, and Mariusz Zdanowicz.

✉ S. S. A. Obayya
sobayya@zewailcity.edu.eg

[1] Electrical Engineering Department, Faculty of Engineering at Shoubra, Banha University, Cairo, Egypt

[2] Centre for Photonics and Smart Materials, Zewail City of Science and Technology, Sheikh Zayed District, 6th of October City, Giza, Egypt

[3] Radiation Engineering Department, National Centre for Radiation Research and Technology (NCRRT), Atomic Energy Authority, Nasr City, Cairo 11787, Egypt

[4] Faculty of Engineering, Mansoura University, Mansoura, Egypt

Published online: 09 January 2017

plasmonic-type sensor in the Kretschmann configuration is presented using the proposed FFT-BPM to ensure its validity in studying such subwavelength-based phenomenon.

Keywords Electromagnetic optics · Goos–Hanchen shift · Optical sensor · Total internal reflection · Numerical/analytical modeling

1 Introduction

The existence of a lateral shift in total internal reflection is attributed, historically, to Newton (1952). Newton reported a theoretical basis and experimental evidence for the penetration of the light into the rarer medium due to the condition of total internal reflection. However, Newton explained the lateral shift with a mechanical model, whereas the Goos–Hanchen (GH) effect is intrinsically due to the wave nature of the electromagnetic radiation field. However, based on the quantum mechanics, the GH effect is attributed to the wave nature of the matter. It is worth to note that the GH-shift has been studied with relative accuracies long time ago (Antar and Boerner 1974; Horowitz and Tamir 1969; McGuirk and Carniglia 1977). The papers of (Lotsch 1970; Puri and Birman 1986) contain references to a large number of both theoretical and experimental studies of the Goos–Hänchen effect in acoustics, nonlinear optics, absorbing media, spatially dispersive media, plasmas, semiconductors, super lattices, etc.

In the recent developments of evanescent-wave sensors (Hoa et al. 2007), near-field plasmonics (Kawata et al. 2009), probing and spectroscopy (Courjon 2003; and Baida et al. 2000), ultra high-density optical multiplexers and de-multiplexers (Van Uden 2014), the spatial features of these objects and the propagation distances of the optical beams should be of the order of the wavelength or much smaller (Fillard 1996). However, most of the studies were limited to large values of the ratio W/λ (≥ 10), where W is half of the total *1/e* width of the beam and λ is the wavelength (Antar 1977). Moreover, some methods—though accurate—were limited to angles of incidence which are not exactly at the critical one (Brekhovskikh and Godin 2013). On one hand, the stability and complexity of the numerical implementation of these methods limit their extension to the domain of near-field structures and subwavelength phenomena (Wang et al. 2016). On the other hand, most of these methods suffer from the difficulties associated with diffractive fields at the subwavelength scales (Makris and Demetri 2011). Additionally, almost all of these methods can't handle inhomogeneous media (Bliokh and Aiello 2013). Accordingly, the invention of a revolutionary method to circumvent the above mentioned difficulties become an exigent demand.

The Beam Propagation Method (BPM) meets, so far, the needs of most of the previously mentioned research areas (Sujecki 2014). The versatility of the BPM ranked it at the top of the numerical methods which are able to handle a broad class of applications in photonic integrated devices, nano-optical devices, plasmonics, near-field optical probing and sensors (Lifante 2015). The accuracy and efficiency of the BPM in a large class of optical phenomenon has been proved, compared to other techniques such as finite difference time domain (FDTD), Finite Element method (FEM), etc. (Sujecki 2014). The bidirectional BPM succeeded to take into account the back reflected fields encountered in many devices especially: laser cavities (Rao et al. 2000), frustrated total internal reflection, and butt-coupling of light beams to wave-guiding structures (Okamoto 2006).

In this paper, the applicability of the BPM in studying the GH shift of optical beam at critical incidence on a dielectric interface and the Kretschmann-type plasmonic sensor is studied and analyzed. Further, the subwavelength rectangular pulse excitation of plasmonic waveguides is considered for the first time to the best of our knowledge. The extension of the FFT-BPM is also reported to investigate a severe case of TM field at an abrupt discontinuity of the refractive index profile. It is shown that by a proper derivation of an *equivalent-index* profile, the TM problem can be transformed to an equivalent TE one, where the usual FFT-BPM could be implemented very easily.

2 Theoretical model and analysis of the interface problem

2.1 TE Gaussian beam

Figure 1 shows an incident Gaussian beam on a plane of dielectric interface between two medium of refractive indices n_1 and n_2 where $n_1 > n_2$. For the sake of simplicity, a 2D structure is assumed (i.e. $\partial/\partial y = 0$) as shown in Fig. 1. A Gaussian beam with its electric field $E_y(x,z)$ parallel to the interface at $x = 0$ is incident at the critical angle $\theta_c\left(= \sin^{-1}(n_2/n_1)\right)$. Further, the axis of the incident beam is located at $x = x_c$. The half-width of the Gaussian beam and the free space wavelength are taken as W and λ_0, respectively.

The incident beam can be expressed as a superposition of plane waves with varying amplitudes. Each component of the plane waves will be reflected from the boundary at $x = 0$ with the proper Fresnel reflection coefficient with different amounts of phase shifts. The reflected beam is formed by incorporating the reflected plane-wave components. Therefore, a lateral shift occurs in the reflected beam. Lotsch (1968) explained that the energy redistribution in the reflected beam takes place to produce a shifted beam, In this regard, he calculated the Poynting vector, which gives the direction of energy flow. It has been shown that a part of the beam indeed enters the rarer medium and reemerges at another point to produce the observed shift.

In the coordinate system (x_i, z_i) the transverse distribution of the E_y component with unity amplitude is written as:

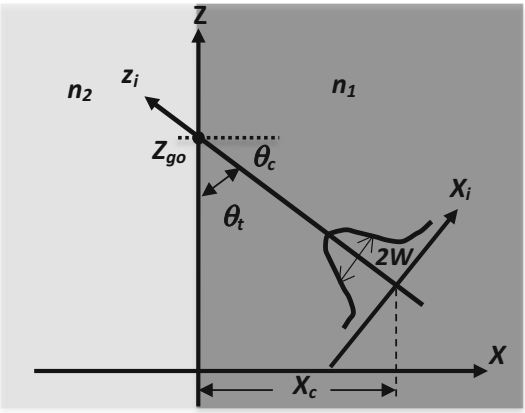

Fig. 1 Incident Gaussian beam on a plane dielectric interface separating two media with refractive indices n_1 and n_2

$$E_y(x_i) = e^{-\left(\frac{x_i}{W}\right)^2} \tag{1}$$

In the (x, z) coordinate system, with the time dependence $exp(j\omega t)$, the Gaussian distribution takes the form (Horowitz and Tamir 1969):

$$E_y(x,z) = e^{-\left[\frac{x-x_c}{W}\cos\theta_t\right]^2 + jkx\sin\theta_t} \tag{2}$$

where θ_t is the "tilt" angle of the beam's axis with respect to the z-axis, and $k = 2\pi n_0/\lambda_0$ is the wavenumber in a reference medium with refractive index n_0. In this study, n_0 is taken as the refractive index of the first medium n_1. Obviously, the refractive index is invariant with respect to z and hence the scalar wave equation for the TE case is written as (Okamoto 2006):

$$\left[\nabla^2 + \mathrm{k}_0^2 n^2(x)\right] E_y(x,z) = 0 \tag{3}$$

where $\nabla^2 \equiv \left(\frac{\partial^2}{\partial x^2}\right) + \left(\frac{\partial^2}{\partial z^2}\right)$. The wide-angle BPM formalism was developed by Feit and Fleck (1978). A FORTRAN program is implemented for the TE case. The marching procedure of the field $E_y(x, z)$ from z to z + Δz is represented as follows:

$$E_y(x, z+\Delta z) = \{P.Q.P\} E_y(x,z) \tag{4}$$

where the propagator and phase correction operators are given as (Feit and Fleck 1978):

$$P = e^{-j\frac{\Delta z}{2}\frac{\nabla_\perp^2}{\sqrt{\nabla_\perp^2 + k^2} + k}} \tag{5a}$$

$$Q = e^{(-j\chi\Delta z)} \tag{5b}$$

where $\nabla_\perp^2 \equiv (\frac{\partial^2}{\partial x^2})$, $k = k_0 n_0$ and $\chi = k_0(n(x) - n_0) = k_0\delta n(x)$. The propagation in the uniform (reference) medium is performed in the spatial-frequency domain (k_x-domain) via Fast Fourier Transform (FFT). However, the phase correction operator Q is applied in the space domain.

In the propagation part of the BPM, the field is decomposed into plane wave components where each plane wave is multiplied by its corresponding plane wave propagator as reported by Feit and Fleck (1978). This is followed by a phase correction applied in the space domain. We consider the value of $(W/\lambda) = 10$, where $\lambda = \lambda_0/n_1$. This case was previously studied by (Antar 1977). Figure 2 represents the contour plot of the total field during its propagation when $\lambda_0 = 1.55$ µm, $n_1 = 1.94$, $n_2 = 1.0$, and $x_c = 5w$. It may be noted from this figure that the peak value of the lateral field along the z-axis in the interface plane x = 0 is displaced by an amount S from the geometrical-optics point of incidence Z_{go} shown in Fig. 1. Around the critical angle of incidence, an approximate analytical expression for the GH-shift has been derived by Antar (1977) and Horowitz and Tamir (1969) as:

$$S_{HT} = \frac{A(\theta)}{2^{5/4}\cos\theta}\mathrm{Re}\left\{\left(\frac{W}{k}\right)^{1/2}\frac{e^{j\pi/4}e^{\left(\gamma_o^2/4\right)}D_{-1/2}(\gamma_o)}{1 + A(\theta)\left[\sqrt{-\delta} - \frac{\sqrt{2}e^{j\pi/4}}{\sqrt{kW}}e^{\left(\gamma_o^2/4\right)}D_{1/2}(\gamma_o)\right]}\right\} \tag{6}$$

where $D_{\pm 1/2}(\gamma_o)$ is the parabolic cylinder function of order (±1/2) and argument γ_o, Re denotes the real part of the evaluated expression and the other functions are defined as follows:

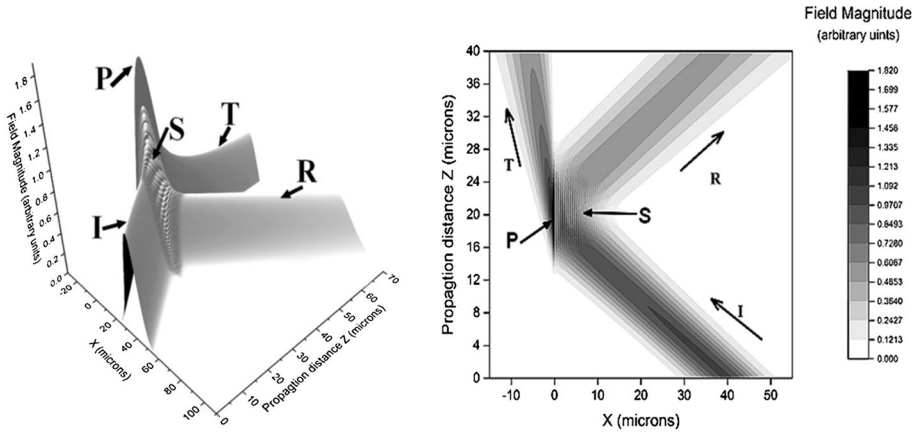

Fig. 2 Total propagated field due to an incident Gaussian beam on a dielectric interface at the critical angle. **I**, **T** and **R** are the launched Gaussian field, transmitted and reflected fields, respectively. **P** and **S** depict the peak field at the interface plane and the standing wave pattern, respectively in the vicinity of the incidence zone on the plane x = 0

$$A(\theta) = 4m\cos^2\theta_c \times \frac{\sin\theta}{\sqrt{\cos\theta(\sin\theta + \sin\theta_c}\left[\cos^2\theta + m^2(\sin^2\theta - \sin^2\theta_c)\right]}$$
$$\delta = \sec\theta(\sin\theta - \sin\theta_c) \tag{7}$$
$$\gamma_o = \frac{jk_1 W\delta}{\sqrt{2}}$$

The constant m depends on the polarization state of the incident beam where $m = 1$ for TE polarization and $m = (n_1/n_2)^2$ for TM case. The wave number in medium 1 is $k_1 = 2\pi n_1/\lambda_o$, where λ_o is the free space wavelength. The above expression S_{HT} for the GH-shift suffers from two main discrepancies. Firstly, as θ approaches θ_c, the parabolic cylinder functions $D_{\pm 1/2}(\gamma_o)$ varies essentially with $(\theta - \theta_c)^{1/2}$ with quasi-infinite slope and a cusp-like structure at the critical angle. Secondly, away from θ_c, S_{HT} is reduced exactly to the well-known classical result of Artmann (1948):

$$S_A = 2m\cos^2\theta_c \times \frac{\sin\theta}{k\sqrt{(\sin^2\theta - \sin^2\theta_c)}\left[\cos^2\theta + m^2(\sin^2\theta - \sin^2\theta_c)\right]} \tag{8}$$

In this study, the lateral shift S is calculated by the FFT-BPM. Figure 3 shows the lateral field along the interface at x = 0 for TE polarization and compared with that obtained by Antar and Boerner (1974). Then, the shift between this field and the incident one for a Gaussian TE beam at the critical incidence is obtained. It is revealed from the figure that a good agreement between the two curves where S/W is almost 0.1. The shift is normalized to the Gaussian beam half-width W. For the sake of clarity, we take the point Z_{go} as the origin of Fig. 3.

2.2 TM Gaussian beam

The difficulties of the BPM with TM field are obvious (Vassallo 1997), especially when the structure under consideration exhibits an abrupt discontinuity in the refractive index profile

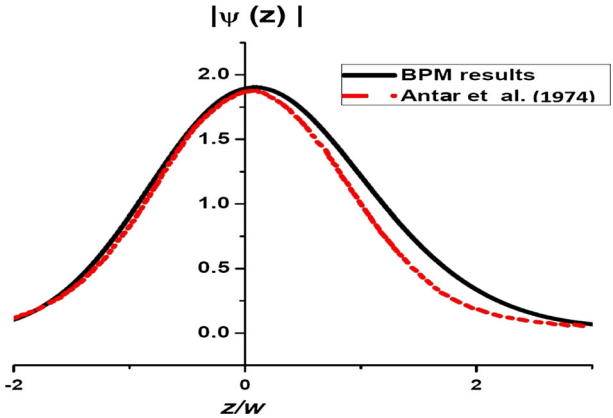

Fig. 3 The Lateral field along the z-axis at x = 0 for TE polarization case

in the transverse direction (x-axis). As pointed out by Poladian and Ladouceur (1998), the scalar wave equation for the magnetic field $H_y(x, z)$ corresponding to the TM case takes the following form (Poladian and Ladouceur 1998):

$$\nabla^2 \mathrm{H}_y(\mathrm{x,z}) + \mathrm{k}_0^2 n^2(x)\mathrm{H}_y(\mathrm{x,z}) - \frac{1}{n^2}\frac{\partial n^2}{\partial x}\frac{\partial H}{\partial x} = 0 \tag{9}$$

Obviously, the last term, $\left(\frac{\partial n^2}{\partial x}\right)\left(\frac{\partial H}{\partial x}\right)$ represents a major problem from the numerical point of view. However, this mixed term, could be avoided by transforming the problem from the TM to an "equivalent" TE with an "equivalent" index given by (Poladian and Ladouceur 1998):

$$n_{eq}^2(x) = n^2(x) - \frac{n(x)}{k_0}\frac{\partial^2}{\partial x^2}\frac{1}{n(x)} \tag{10}$$

Accordingly, the TM problem is reduced to an equivalent TE one, where the scalar wave equation is converted to:

$$[\nabla^2 + \mathrm{k}_0^2 n_{eq}^2]F(x,z) = 0 \tag{11}$$

Where $F(x,z) = H_y(x,z)/n(x)$. However, the transverse second derivative of the $1/n(x)$ in Eq. 10 still a major problem (in the equivalent TE-BPM) since the profile $n(x)$ has a step-like shape at $x = 0$. Yamauchi et al. (2009) proposed a sigmoide function of the form:

$$n(a,x) = n_2 + \frac{\delta n}{1 + e^{-(a/x)}} \tag{12}$$

to approximate a step-like interface between two half-spaces n_2 and $n_2 + \delta n$, where "a" a parameter that describes the "steepness" of the index change at the interface $x = 0$. This function is used to approximate the step-index profile at the interface for the TM case. However, the parameter "a" should be large (≥500) (Yamauchi et al. 2009) in order to approach as close as possible the actual abrupt index change at $x = 0$.

Clearly, for an abrupt index change, the second derivative in Eq. 10 $\left(\frac{\partial^2}{\partial x^2}\frac{1}{n(x)}\right)$ is singular and must be replaced by $\frac{\partial^2}{\partial x^2}\frac{1}{n(a,x)}$ with n (a, x) as given in Eq. 12. Numerically, very large

and sharp spikes (for $a \geq 500$) appear in the equivalent index when $n(x)$ is substituted with $n(a, x)$ from Eq. 12. Such spikes lead to a numerical diverging behavior, and hence the equivalent TE-BPM becomes impossible, unless "a" is reduced to much lower values than 10^4. However, this reduction in a degrades the accuracy of the equivalent TE-BPM. In evaluation the values of GH shift and the lateral shift of interface field.

In this paper we proposed another function to solve the ambiguities associated with the sigmoid function. An *arc-tangent* function was successful in the approximation of the abrupt change in the refractive index at $x = 0$. The step-like index profile at $x = 0$ is, therefore, approximated by:

$$n_{arc}(x) = n_2 + \left\{ \delta n \left[0.5 + \frac{\tan^{-1}(x/a)}{\pi} \right] \right\} \tag{13}$$

where the parameter "a" could be kept as small as required of order 1 nm or less to describe the degree of steepness in $n(x)$ from n_2 for $x < 0$ to $n_1 = n_2 + \delta n$ where $x \geq 0$. As a decrease to zero, the $n_{arc}(x)$ tends to a perfect step change from n_1 for $x \geq 0$ to n_2 for $x < 0$. Inserting Eq. 13 into Eq. 10, we get the equivalent index profile n_{eq}^2 as:

$$n_{eq}^2(x) = n_{arc}^2 - \frac{n_{arc}(x)}{k_0} \left[\frac{2(\delta n)^2}{n_{arc}^3(x) \cdot \pi^2 a^2 \cdot (1 + \frac{x^2}{a^2})^2} + \frac{2x\delta n}{n_{arc}^2(x) \cdot \pi a^3 \cdot (1 + \frac{x^2}{a^2})^2} \right] \tag{14}$$

The equivalent n_{eq} is then substituted in Eq. 11 and an equivalent TE-BPM is implemented with the same parameters as those considered previously in Fig. 3. The lateral field is plotted in Fig. 4 at steepness $a = 0.05$ μm and compared with that one obtained by Antar and Boerner (1974). It is revealed from this figure that a good agreement between the results of the two methods is achieved.

2.3 Rectangular spatial pulse

The ability of the BPM to tackle challenging problems is tested by considering a rectangular spatial pulse of width $W = 10\lambda = 10\ \lambda_0/n_1$ centered at $x_c = 40$ μm from the interface at $x = 0$. An overall evolution of the total propagated field is shown in Fig. 5a, b. The

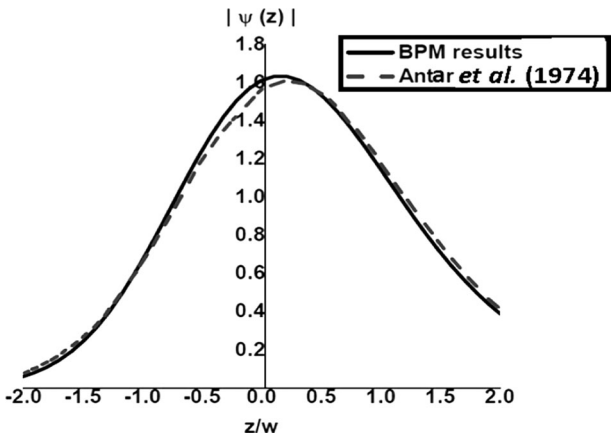

Fig. 4 The lateral field along the z-axis for the TM polarization case at a = 0.05 μm

rectangular pulse P is launched at z = 0 with its axis tilted at an angle $\theta_t = 59°$ with respect to the z-axis which corresponds to the critical angle of incidence $\sin^{-1}\left(\frac{1}{1.94}\right) = 31°$ on the interface at $x = 0$. The geometrical optical point of incidence is taken as $Z_{go} = -x_c/\tan\theta_t = 24$ µm. At the interface, a peak spot "S" occurs similar to the Gaussian beam case. This peak is shifted from the point Z_{go} by an amount equals to the shift exhibited by the lateral field as shown in Fig. 6. The lateral field of the Gaussian beam is also shown in Fig. 6 for the purpose of comparison.

The lateral shift of the rectangular pulse $(z - z_{go})/w = 0.64$ is six times greater than that of the Gaussian beam with a shift of 0.1. This is expected since the spectral extent of

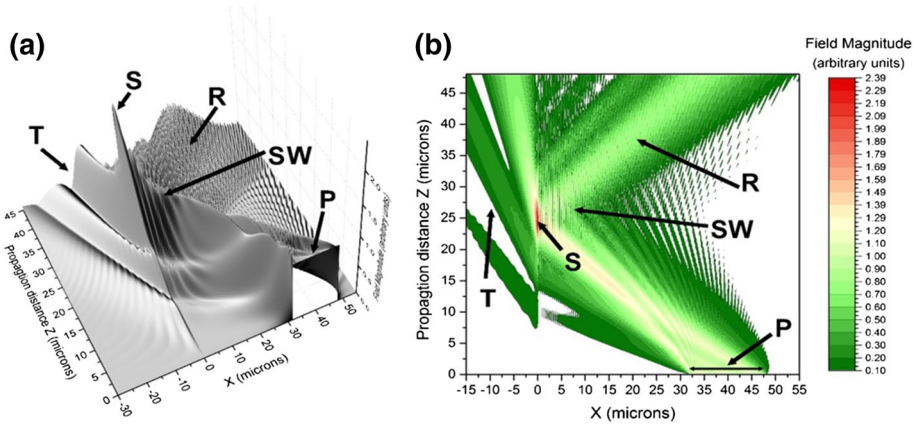

Fig. 5 The total propagated field due to a launched rectangular pulse P, while, T and R are the transmitted and reflected fields. The peak of the lateral field S at the interface plane and SW is the standing wave pattern in the vicinity of the incidence zone on the plane x = 0, (**a**) 3D plot and (**b**) contour plot

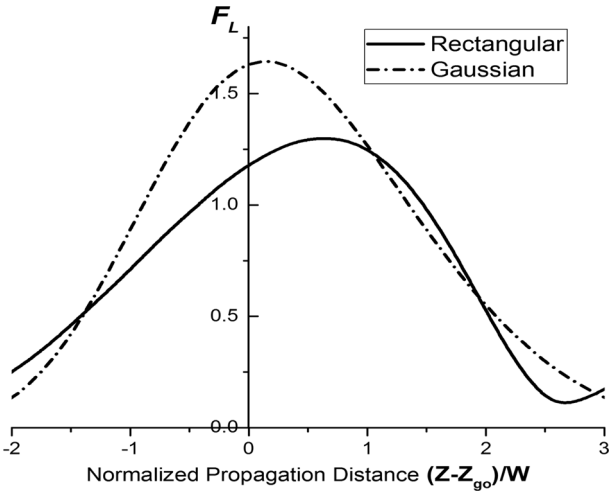

Fig. 6 A rectangular pulse launched in the plane z = 0 creates a lateral field FL along the z-axis. The lateral shift is 6 times greater than the corresponding one for a Gaussian beam

the rectangular pulse of width W in the spectral k_x-*space* is proportional to $2W(\sin k_x W)/k_x W$. However, the spectrum of a Gaussian shape of the same width (W) in the k_x-*space* is proportional to $\sqrt{\pi} W e^{-k_x^2 W^2/4}$. An elementary justification is obvious if we note that the (1/e) width of a Gaussian spectrum is $k_{x_g} = 2/W$ while that of the sinc-function (The spectrum of a rectangular pulse) is roughly $k_{x_p} = \pi/W$ (the first null of the sinc-function). Accordingly, the amount of plane wave spectral components contributing to the lateral shift of the rectangular pulse is larger than those contributing to the lateral shift of the Gaussian beam by an amount $\approx k_{x_p}/k_{x_g} \sim (\pi/2)$ (i.e. approximately 160%).

It is well known that the lateral shift of an optical beam is proportional to the divergence angle (angular spread) $\Delta\theta_t$ of the beam. The divergence angle $\Delta\theta_t$ of the rectangular pulse could be estimated from the extent of the plane wave spectral components of the spatial spectrum (i.e. in the k_x-space) of the pulse. It is straightforward to evaluate $\Delta\theta_t$ since the axis of the pulse is tilted with an angle $\left(\frac{\pi}{2} - \theta_c\right) = 59°$ with respect to the z-axis. The corresponding spectral wavenumber is $k_{x0} = k_0 n_1 \sin\theta_t = 6.74\ \mu\text{m}^{-1}$. Taking into account the spectral extent of the pulse $k_{x_p} = (\pi/W) = 0.785\ \mu\text{m}^{-1}$, we can see that the pulse's spectrum extends in the k_x-space by an amount: $k_{x0} \pm k_{xp} = k_0 n_1 \sin\theta_c \pm \pi/W = (6.74 \pm 0.785)\ \mu\text{m}^{-1} = 7.525$ to $5.955\ \mu\text{m}^{-1}$. This spectral extent corresponds to an angular extent from $\sin^{-1}(5.955/k_0 n_1)$ to $\sin^{-1}(7.525/k_0 n_1)$ i.e. from 49.2° to 73.1°. This amounts to an angular spread $\Delta\theta_t = 24°$ around the direction of the axis of the rectangular pulse which makes 59° with respect to the z-axis. Such a relatively large angular spread is responsible for the large lateral shift associated with the lateral interface field as depicted in Fig. 6.

It should be pointed out that the shape of the launched rectangular pulse evolves significantly in the vicinity of the launching plane $z = 0$. Figure 7a, b depict such evolution, where the left side of the pulse facing the interface at $x = 0$, exhibits ripples; while the right side is apparently not affected too much.

The spatial period of these ripples is "not uniform" and it varies from 1.45 μm at the left side of the pulse to almost 0.6 μm near the right side of the pulse. Here, we could mention that the exact analysis of the evolution of the shape of a spatial-limited light beam needs a consideration from the interested researchers. We claim that these ripples are a manifestation of a certain kind of a quite complex diffraction phenomenon associated with

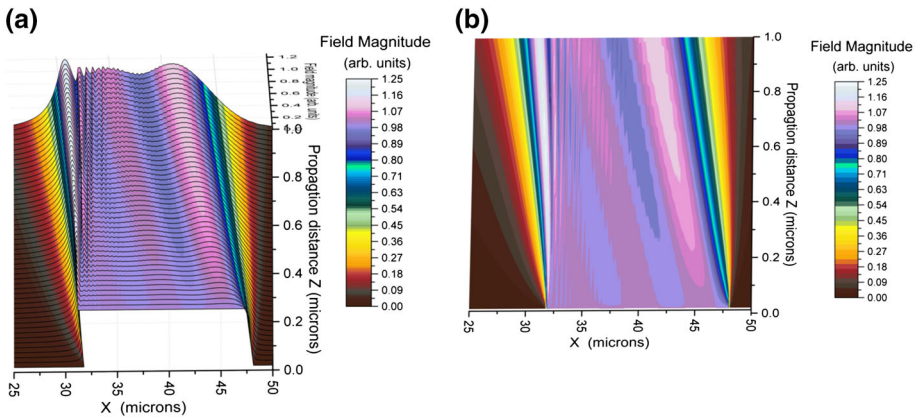

Fig. 7 Evolution of the rectangular pulse shape in the vicinity of the launching plane z = 0, **a** 3D plot and **b** contour plot

the spatial transient of the pulse edges. This behavior is very similar to the diffraction of a plane wave by a slit in a conducting plane; as will be explained now.

2.3.1 Spatial transients and the diffraction phenomenon

Let us consider the radiation from a slit width with the same width of the rectangular pulse used in the BPM calculations (20 λ_1) as shown in Fig. 8.

In this study, a uniform plane wave with unity-amplitude: e^{-jkZ} is incident from the left of the slit. The far field is observed at a distance Z from the slit, using the approximate Fresnel diffraction formula as:

$$E(x,z) = \sqrt{\frac{jk}{2\pi z}} e^{-jkz} \int_{-a}^{a} e^{jk(x-x')^2/2z} dx' \tag{15}$$

The integral is evaluated in terms of Fresnel-Integrals as:

$$E(x,z) = \sqrt{\frac{jk}{2}} e^{-jkz} \cdot \left[\mathbb{F}\left(\sqrt{\frac{2}{\lambda z}}(-x+a) \right) - \mathbb{F}\left(\sqrt{\frac{2}{\lambda z}}(-x-a) \right) \right] \tag{16}$$

where the Fresnel-integral F is given in terms of the cosine and sine integrals:

$$\mathbb{F}(\mathrm{u}) = C(\mathrm{u}) - jS(\mathrm{u}) = \int_0^u \cos\left(\frac{\pi v^2}{2}\right) dv - \int_0^u \sin\left(\frac{\pi v^2}{2}\right) dv \tag{17}$$

The Fresnel-integrals are calculated numerically via a FORTRAN program, and the diffraction pattern is evaluated at Z = 1000 μm. Figure 9 shows the field magnitude calculated by the Fresnel-integrals and the suggested FFT-BPM. It is revealed from this figure that an excellent agreement between both results is achieved.

The far-field at a distance $Z \geq (2a)^2/(\lambda/2)$ (the Rayleigh distance) can be regarded as the diffraction from two knife edges at x = ±a. An elementary result from the antenna theory shows that the first nulls of the far-field pattern (the Sinc-function) occur at an angle of $\theta_o = sin^{-1}(\lambda/2a)$. Therefore, the two lines making this angle with the Z-axis give the directions of the two nulls of the main lobe as shown in Fig. 10. Accordingly, at the end of the propagation distance Z = 1000 μm, the first nulls occur at $X = \pm$ Z tan ($\sin^{-1}(\lambda/2a) = \pm 1000 \tan[\sin^{-1}(1/20)] = \pm 50$ μm. This justifies our claim that the pulse propagation is due to the diffraction of a plane wave by a slit. In the near-zone, the *ripples* occur at the beginning of the propagation process. Figure 11 shows the evolution of the rectangular pulse shape during the propagation (using the BPM) over a distance of 0.8 μm in the medium n_1 with $n_1 = 1.94$ and the free space wavelength $\lambda_o = 1.55$ μm).

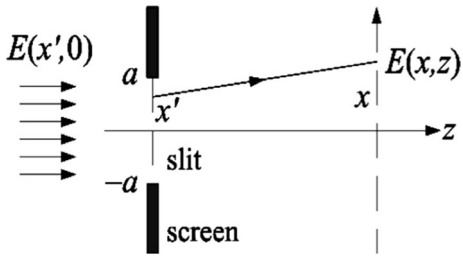

Fig. 8 Slit analogous to the rectangular pulse

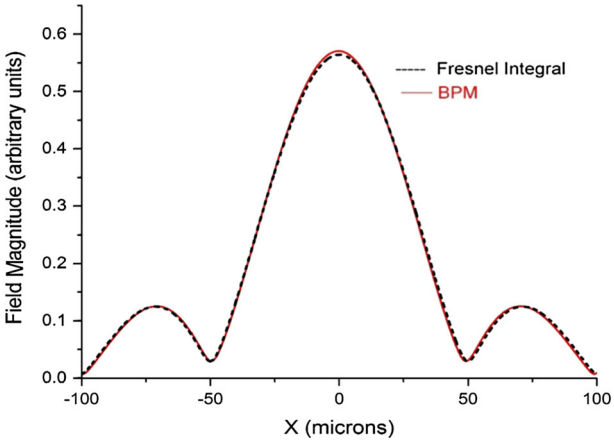

Fig. 9 Far field of a plane wave diffracted by a slit, and rectangular pulse propagated a distance Z = 1000 μm in a uniform homogeneous medium

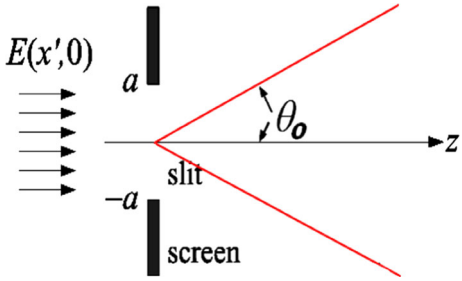

Fig. 10 The two lines giving the directions of the two nulls of the main lobe along Z direction

The analytical results based on Huygens' principle leading to Fresnel-integral are not accurate close to the aperture (Goodman 2005), this is due to the assumption based on the physical-optics at which the aperture field is the same as the incident field. Further, the vanishing fields over the conducting screen do not satisfy the boundary conditions. However, Sommerfeld solution of the plane wave diffraction by a perfectly conducting half-plane has been used extensively to synthesize the diffraction of an incident plane wave on a slit due to the diffraction of two interacting half-planes. The diffraction ripples in the near field (Fresnel-region) can thus be viewed due to a complicated interference between the simple geometric-optical field transmitted through the aperture, and the cylindrical edge waves scattered from the two edges of the slit. Accordingly, we can calculate the near-field diffraction pattern in the Fresnel-zone (which extends till $Z \leq (2a)^2/3\lambda$, i.e. $\leq$16 μm) by the diffraction integral:

$$E(x,z) = \sqrt{\frac{jk}{2}} e^{-jkz} \cdot \left[\mathbb{F}\left(\sqrt{\frac{2}{\lambda z}}(-x+a) \right) - \mathbb{F}\left(\sqrt{\frac{2}{\lambda z}}(-x-a) \right) \right] \tag{18}$$

Figure 12 depicts the results obtained from the BPM and Fresnel-integral when Z = 16 μm. It may be noted from Fig. 12 that the ripples occur in both cases. Therefore, it can be concluded that such ripples exist due to diffraction effects.

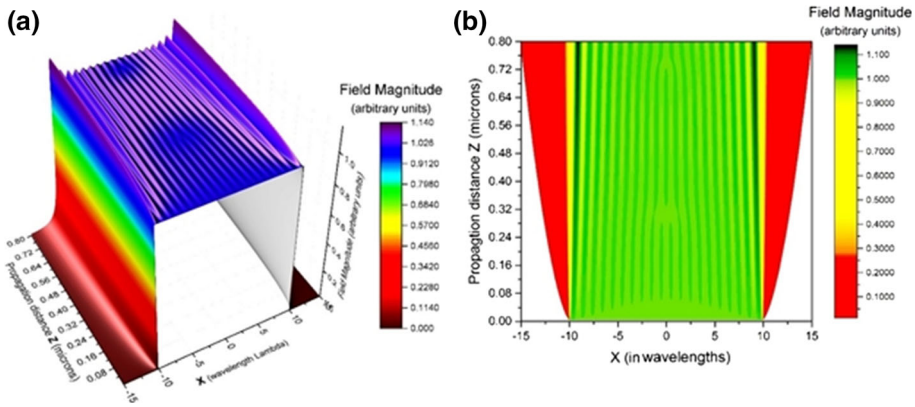

Fig. 11 Ripples formation over the width of the rectangular pulse from the beginning of the propagation process **a** 3D plot and **b** contour plot

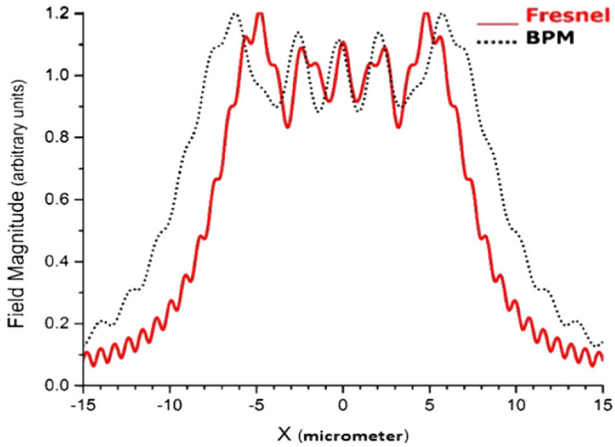

Fig. 12 Ripples formation along the width of the propagated rectangular pulse and the diffraction pattern of the radiation from the slit as calculated by Fresnel integral in the near-zone at a distance 16 μm from the slit

2.3.2 Standing wave effects

The interference between the incident pulse and the reflected field results in a standing wave (*SW*) field near the peak of the lateral field *S* as shown in Fig. 5. Such a standing wave field is depicted in the closer shot of Fig. 13a, b.

The standing wave field variation from the peak spot *S* with the distance in the positive *x* distance for a distance of 5 μm is shown in Fig. 14, it may be seen from this figure that the periodicity of that pattern is about 0.478 μm. It is worth noting that the rectangular pulse has a spectral extent in the k_x-space from 5.955 to 7.525 μm^{-1}. This corresponds to an *x*-wavelength "λ_x" ranging from $(2\pi/7.525) = 0.835$ μm to $(2\pi/5.955) = 1.055$ μm. Therefore, the average *x*-wavelength is $\lambda_{xav} = 0.5(0.835 + 1.055) = 0.945$ μm. Further,

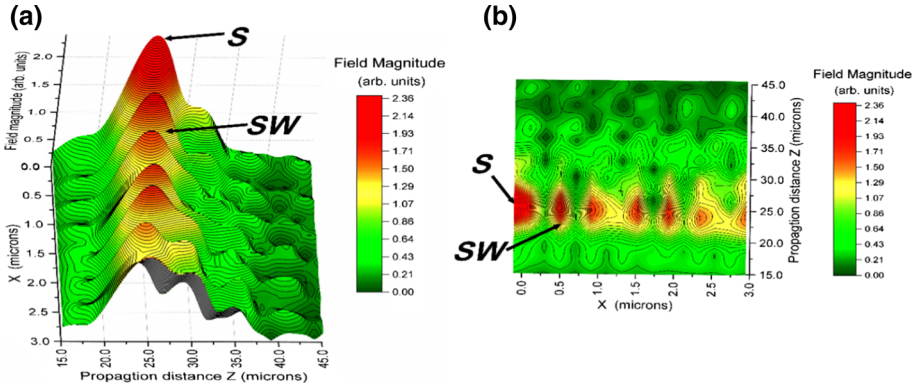

Fig. 13 **a** 3D Plot of the standing wave pattern *SW* in the vicinity of the interface peak spot *S* and **b** The corresponding contour plot

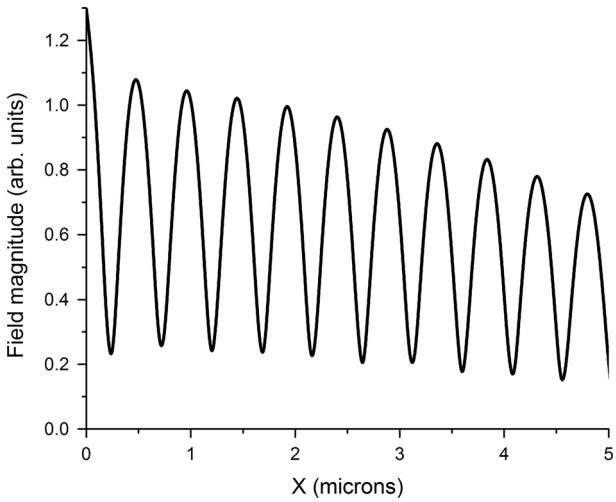

Fig. 14 The field variation from the peak of spot zone S as we move away from the interface for a distance of 5 μm

the standing wave pattern shown in Fig. 14 has a period of 0.5 $\lambda_x = 0.478$ μm, where, $\lambda_x \approx 0.956$ μm. This value agrees perfectly (to within 1%) with the above mentioned value $\lambda_{xav} = 0.945$ μm.

2.3.3 Parametric study of Kretschmann-type plasmonic sensor

In order to ensure the usefulness of the proposed FFT-BPM, a parametric study of plasmonic sensor based on Kretschmann configuration is investigated as shown in Fig. 15. In this study a prism of refractive index $n_1 = 1.5$ is placed over a silver film of thickness d = 60 nm and refractive index $n_2 = 0.06$-j4. Further, the incident light has a wavelength of 0.633 μm and the propagation length is taken as 0.6 μm. The metallic film allows the plasmons to travel along the nanoscale metallic guiding film, and hence, direct coupling of optical signals to nanometer electronic devices can occur (Peale et al. 2016). Figure 16

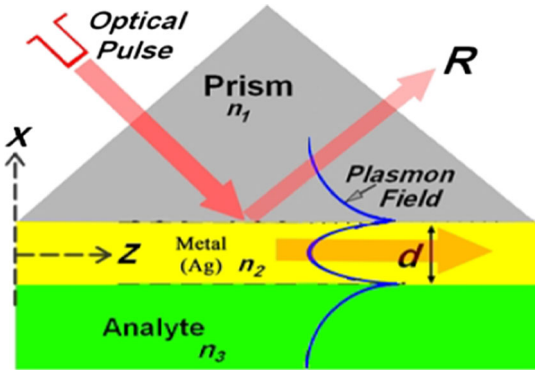

Fig. 15 Kretschmann-type Surface Plasmon (SP) sensor

shows the propagation of an incident sub-wavelength pulse of width λ/4 through the studied configuration with analyte refractive index $n_3 = 1$. The parameter "a" is set to 0.1 of the computational step size in the x-direction which amounts to 0.025 nm. The effects of the analyte refractive index n_3 and the light wavelength λ on the guided power carried by the plasmonic field are investigated.

2.3.4 Sensitivity Study

A subwavelength TM rectangular pulse with a width of λ/2 where $\lambda = 0.63//n_1$ μm is incident on the base of the prism at the critical angle sin^{-1} (n_3/n_1). The narrow pulse has a wide plane wave spatial spectrum that can excite the plasmonic waveguide modes which propagate along the metallic film. The guided power P_g which is proportional to the integral: $\int_{-d/2}^{d/2} |H_y(x)|^2/n^2(x)dx$ is calculated at the end of the propagation distance of 3 μm. In this study, the analyte refractive index n_3 is changed from 1 to 1.5 at different film thicknesses 20, 40 and 60 nm as shown in Fig. 17. It may be noted from this figure that the peak of the normalized guided power increase by decreasing the film thickness. Further,

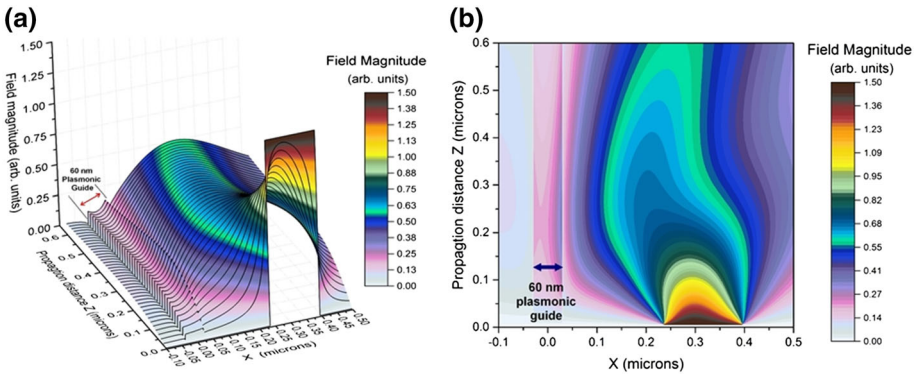

Fig. 16 3D and contour plots of an incident quarter-wavelength pulse width on a 60 nm plasmonic guide via evanescent wave coupling in the Kretschmann configuration with λ = 0.63 μm, prism index = 1.5, and air as an analyte

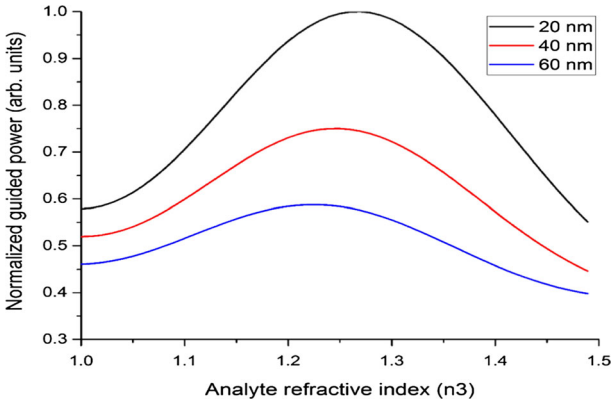

Fig. 17 Sensitivity curves of Kretschmann-type sensor for three different values of the film thickness: 20, 40 and 60 nm

the peaks are shifted toward the upper analyte refractive index $n_3 = 1.5$ by decreasing the film thickness. This could be predicted theoretically, since the plasmons at the sides of the thinner films (facing the prism and the analyte) interact stronger than the thicker films (where the plasmons are separated further apart). Therefore, more power could be launched to thinner films than the thicker ones (Sarid 1981; Berini 2009).

2.3.5 Spectral response

The amount of the guided plasmonic power varies with the wavelength of the incident light pulse on the base of the prism. Figure 18 depicts such variation in the wavelength range from 0.4 to 0.7 μm. The prism and analyte refractive indices are kept constants at 1.5 and 1 respectively, while the film thickness changes from 20 to 60 nm as shown in Fig. 18. The Drude model is used to calculate the relative permittivity of the silver film as follows (Johnson and Christy 1972):

$$\varepsilon_2(\omega) = 1 - \frac{\omega_p^2}{\omega^2 + j\omega\gamma} \tag{19}$$

where the plasma angular frequency $\omega_p = 1.326 \times 10^{16}$ rad/s, and the phenomenological electron's relaxation frequency $\gamma = 7.055 \times 10^{15}$ rad/s. It may be seen from Fig. 18 that

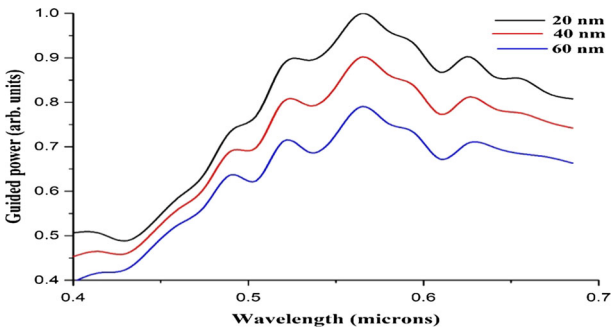

Fig. 18 Spectral response curves of Kretschmann-type sensor at different values of the film thickness *d*

the peak response occurs at $\lambda = 0.565$ μm regardless the value of d (the film thickness). Also, the amount of the guided power increases by decreasing the film thickness which is compatible with the results of the sensitivity analysis.

3 Conclusion

In this paper we presented the results of studying some types of optical beams interacting with a dielectric interface at critical angle of incidence. Our aim is to demonstrate the competitiveness of the FFT-BPM in the investigation of a relatively wide class of optical beam propagation and interaction. Firstly, to demonstrate the conformity of the results obtained by the BPM with other well-known approximate methods (Antar and Boerner 1974; Horowitz and Tamir 1969; McGuirk and Carniglia 1977). We studied the case of a TE Gaussian beam, and compared the shift of the lateral field with that one obtained by other sophisticated method (relying on a solution involving parabolic cylinder functions). Secondly, we adapted the BPM to treat the TM case involving abrupt refractive index change in a direction transverse to the direction of propagation. The difficulties associated with that delicate case are circumvented via an equivalent-index formalism (proposed by Poladian and Ladouceur (1998)), which transformed the TM problem to an equivalent TE one. The ability of the BPM to tackle propagation problems involving sharp-limited spatial beams is tested by considering rectangular pulse incident on dielectric and metal interfaces (plasmonic waveguides in Kretschmann-type sensor). An analytical justification of the spatial-transient behavior of the propagated pulse is presented. Also, a parametric study involving sensitivity and spectral assessments of the Kretschmann-type sensor is presented.

Compliance with ethical standards

Conflict of interest The authors would like to ensure the objectivity and transparency in the submitted research paper. Additionally, the authors would like to ensure that accepted principles of ethical and professional conduct have been followed through the preparation of the proposed paper. Further, we would like to clarify that there is no sources of funding, and no potential conflicts of interest (financial or non-financial).

Human and animal rights Moreover, the submitter research does not involve human participants, or animals.

References

Antar, Y.M.M.: The transmitted field of a Gaussian laser beam at total internal reflections. Can. J. Phys. **55**, 2023–2035 (1977)

Antar, Y.M., Boerner, W.M.: Gaussian beam interaction with a planar dielectric interface. Can. J. Phys. **52**(11), 962–972 (1974)

Artmann, K.: Berechnung der Seitenversetzung des total reflektierten Strahles. Ann. Phys. **6**(2), 87–102 (1948)

Baida, F.I., Labeke, D., Vigoureux, J.M.: Numerical study of the displacement of a three dimensional Gaussian beam transmitted at total internal reflection. Near- field applications. J. Opt. Soc. Am. A: **17**, 858 (2000)

Berini, P.: Long-range surface plasmon polaritons. Adv. Opt. Photon. **1**(3), 484–588 (2009)

Bliokh, K.Y., Aiello, A.: Goos–Hänchen and Imbert–Fedorov beam shifts: an overview. J. Opt. **15**(1), 014001–014017 (2013)

Brekhovskikh, L.M., Godin, O.: Acoustics of layered media II. Springer, Berlin (2013)

Courjon, D.: Near-Field Microscopy and Near-Field Optics, vol. 317. Imperial College Press, London (2003)

Feit, M.D., Fleck, J.A.: Light propagation in graded-index optical fibers. Appl. Opt. **17**, 3990–3998 (1978)
Fillard, J.: Near Field Optics and Nanoscopy. World Scientific, Singapore (1996)
Goodman, J.W.: Introduction to Fourier optics. Roberts and Company Publishers, San Francisco (2005)
Hoa, X.D., Kirk, A.G., Tabrizian, M: Towards integrated and sensitive surface plasmon resonance biosensors: a review of recent progress. Biosens. Bioelectron. **23**, 151 (2007)
Horowitz, B.R., Tamir, T.: Lateral displacement of a light beam at a dielectric interface. J. Opt. Soc. Am. **61**, 568–594 (1969)
Johnson, P.B., Christy, R.W.: Optical constants of the noble metals. Phys. Rev. B **6**(12), 4370 (1972)
Kawata, S., Inouye, Y., Verma, P.: Plasmonics for near-field nano-imaging and superlensing. Nat. Photon. **3**(7), 388–394 (2009)
Lifante, G.: Beam Propagation Method for Design of Optical Waveguide Devices. Wiley (2015)
Lotsch, H.K.: Reflection and refraction of a beam of light at a plane interface. J. Opt. Soc. Am. A: **58**(4), 551–561 (1968)
Lotsch, H.K.V.: Beam displacement at total reflection: the Goos–Hanchen effect I. Optik **32**(2), 116–137 (1970)
Makris, K., Demetri, P.: Huygens–Fresnel diffraction and evanescent waves. Opt. Commun. **284**(6), 1686–1689 (2011)
McGuirk, M., Carniglia, C.: K.: An angular spectrum representation approach to the Goos–Hänchen shift. J. Opt. Soc. Am. **67**, 103–107 (1977)
Newton, I.: Optiks. Dover, New York (1952)
Okamoto, K.: Fundamentals of Optical Waveguides. Elsevier Inc., Burlington (2006)
Peale, R.E., Smith, E., Smith, C.W., Khalilzadeh-Rezaie, F., Ishigami, M., Nader, N., Vangala, S., Cleary, J.W.: Electronic detection of surface plasmon polaritons by metal-oxide-silicon capacitor. APL Photon. **1**(6), 066103 (2016)
Poladian, L., Ladouceur, F.: Unification of TE and TM beam propagation algorithms. IEEE Photon. Technol. Lett. **10**(1), 105–107 (1998)
Puri, A., Birman, J.L.: Goos–Hänchen beam shift at total internal reflection with application to spatially dispersive media. J. Opt. Soc. Am. A: **3**(4), 543–549 (1986)
Rao, H., Steel, M.J., Scarmozzino, R., Osgood, R.M.: Complex propagators for evanescent waves in bidirectional beam propagation method. J. Lightwave Technol. **18**(8), 1155 (2000)
Sarid, D.: Long-range surface-plasma waves on very thin metal films. Phys. Rev. Lett. **47**, 1927–1930 (1981)
Sujecki, S.: Photonics Modelling and Design. CRC Press, Boca Raton (2014)
Van Uden, R.G.H.: Ultra-high-density spatial division multiplexing with a few-mode multicore fibre. Nat. Photon. **8**(11), 865–870 (2014)
Vassallo, C.: Difficulty with vectorial BPM. Electron. Lett. **33**(1), 61–62 (1997)
Wang, X., Yin, C., Cao, Z.: Progress in Planar Optical Waveguides, pp. 163–189. Springer, Berlin (2016)
Yamauchi, J., Shimada, N., Nito, Y., Hisamatsu N.: Transverse-magnetic BPM analysis of a step-index slab waveguide expressed by a sigmoid function. IEEE Photon. Tech. Lett. **10**(1) (2009)